https://doi.org/10.5194/egusphere-2025-3647
Preprint. Discussion started: 26 September 2025

Microstructure and ice dynamics - Integrating Grain Properties, Fabric, and Borehole Data in the NEEM Ice Core

Miguel Moreno[1], André Lamott[2], Sepp Kipfstuhl[3], Ilka Weikusat[3], María-Gema Llorens[4], Yannick Heiser[1], and Dorthe Dahl-Jensen[1,5]

[1]University of Copenhagen, Physics of Ice, Climate and Earth, Copenhagen, Denmark
[2]Schäfter + Kirchhoff GmbH, Hamburg, Germany
[3]Helmholtz Centre for Polar and Marine Research, Alfred Wegener Institute, Bremerhaven, Germany
[4]GEO3BCN-CSIC , Barcelona, Spain
[5]University of Manitoba, Centre for Earth Observation Science, Winnipeg, MB R3T 2N2, Canada

Correspondence: Miguel Moreno (miguel.moreno@nbi.ku.dk)

Abstract. The physical properties of ice grains, including grain size and orientation, are fundamental to understanding ice flow and deformation processes in polar ice sheets. This study leverages a newly developed large-area scanning microscope (xLASM) and an automated microtome to non-destructively analyze the NEEM ice core's microstructure across 55 cm segments. The resulting microstructural data are compared with continuous flow analysis (CFA) measurements of impurity concentrations, fabric orientation, and shear strain rates over a 16-meter section (2004-2020 m depth) that spans the Last Glacial Maximum and abrupt climatic transitions during Dansgaard-Oeschger event GS-20. Our results reveal strong associations between grain size, impurity concentrations, and shear deformation rates, with impurity-rich, fine-grained stadial ice exhibiting higher shear strain rates. The ice fabric remains stable despite the changes in shear deformation, indicating that, in this case, the fabric is not the cause of the changing deformation.

1 Introduction

The Greenland and Antarctic ice sheets play a critical role in the Earth's climate system as vast reservoirs of frozen water. Over millions of years, these ice sheets have evolved and responded dynamically to climatic shifts, significantly influencing global sea levels and climate patterns. Today, ice sheets are experiencing significant mass loss, with Antarctica and Greenland contributing approximately 150 and 270 Gt of ice per year to rising sea levels, respectively (Otosaka et al., 2022).

Ice cores extracted from these regions provide detailed and continuous paleoclimate records, offering insights into past temperature, precipitation, and atmospheric composition. Since the first deep ice core was drilled at Camp Century in Greenland in the 1960s (Hansen and Langway, 1966), ice core drilling projects have primarily aimed to reconstruct climate history by sampling undisturbed ice that preserves its stratigraphic integrity over millennia. Consequently, most Greenland cores such as GRIP, GISP2, NorthGRIP, and NEEM have been drilled in regions with minimal ice flow (Dansgaard et al., 1993; Grootes et al., 1993; North Greenland Ice Core Project members, 2004; Dahl-Jensen et al., 2013). In Figure 1 a Greenland ice sheet velocity map derived from Sentinel-1 data (Nagler et al., 2015) shows that NEEM and other deep core sites are located in areas

https://doi.org/10.5194/egusphere-2025-3647
Preprint. Discussion started: 26 September 2025

of thick ice and low horizontal flow (e.g., NEEM at 5.8 m/year; Hvidberg et al. (2012)). Beyond paleoclimate reconstruction, ice cores provide essential data for climate and sea-level rise models by capturing ice sheet properties that govern deformation rates, rheology, and flow stability. Modelling these behaviours relies on understanding the microstructural features and small-scale structural elements within the ice, such as grain boundaries, subgrain boundaries, and inclusions, which influence ice mechanics. The EastGRIP ice core project, situated on the Northeast Greenland Ice Stream with flow speeds of approximately 50 m/year (Hvidberg et al., 2020) is the first core location chosen primarily to study ice properties and flow dynamics.

Early laboratory studies of polycrystalline ice, as described by Glen (1952, 1955) and further developed by Nye (1957) in what is now known as the Glen-Nye flow law, used constitutive equations in which the power law relates stress and strain rate with the flow law parameter depending solely on temperature. However, laboratory experiments and detailed ice core analyses significantly advanced the understanding of ice deformation by highlighting the influence of microstructural parameters such as grain size, impurity concentration, and grain fabric variations on ice viscosity and deformation rates (Dahl-Jensen et al., 1997; Durand et al., 2006a; Obbard and Baker, 2007; Baker et al., 2003; Barnes and Wolff, 2004; Iliescu and Baker, 2008; Weikusat et al., 2009; Rhodes et al., 2011; Hammonds and Baker, 2016; Stoll et al., 2021). Experimental work by Duval et al. (1983) and Jacka (1984) identified creep regimes controlled by grain size and dislocation processes, while Pimienta et al. (1988) and Jacka and Jun (1994) demonstrated how impurities and grain-size evolution significantly affect ice rheology, especially in impurity-rich glacial ice. More recently, laboratory experiments by Goldsby and Kohlstedt (2001) further supported that smaller grains promote enhanced deformability through grain-size-sensitive creep mechanisms. New modelling explicitly incorporated microstructural parameters, refining the ice flow models (Azuma, 1994; Kuiper et al., 2020a, b)

Advances in microstructure mapping techniques now allow high-resolution imaging of ice core surfaces, capturing critical features like grain boundaries, inclusions, and subgrain structures (Weikusat et al., 2009, 2011; Eichler et al., 2017; Stoll et al., 2021). This method, initially developed by Kipfstuhl et al. (2006) and refined by Binder et al. (2013); Binder (2014), enables systematic microtoming followed by controlled sublimation to produce detailed 2D ice surfaces. This controlled sublimation reveals fine structural details: sublimation grooves form as etched lines along grain boundaries where ice sublimates more rapidly due to the higher energy state of these boundaries. Our study utilises an enhanced microstructure mapping approach, employing the extra Large Area Scanning Microscope (xLASM), which enables non-destructive imaging of large core sections (up to 55 cm by 10 cm) with a spatial resolution of 5 microns.

This work presents a detailed analysis of a Dansgaard-Oeschger event, specifically DO event GS-20, a rapid millennial-scale climate oscillation during the last glacial period characterised by abrupt warming followed by gradual cooling. For this analysis, we integrate microstructural mapping data with water isotopes, impurity concentrations, fabric, and shear strain measurements. Although many prior studies have focused on the evolution of ice fabric to interpret deformation regimes and derive past strain histories (e.g. Montagnat et al. (2014); Azuma (1994), our results reveal that over a 16-meter section of the NEEM ice core, grain size and impurity variations vary during abrupt climatic transitions while the fabric remains stable. This finding suggests that, in this case, deformation variations are not primarily governed by fabric evolution, but rather reflect the influence of grain size and impurity concentrations on rheological behaviour.

https://doi.org/10.5194/egusphere-2025-3647
Preprint. Discussion started: 26 September 2025

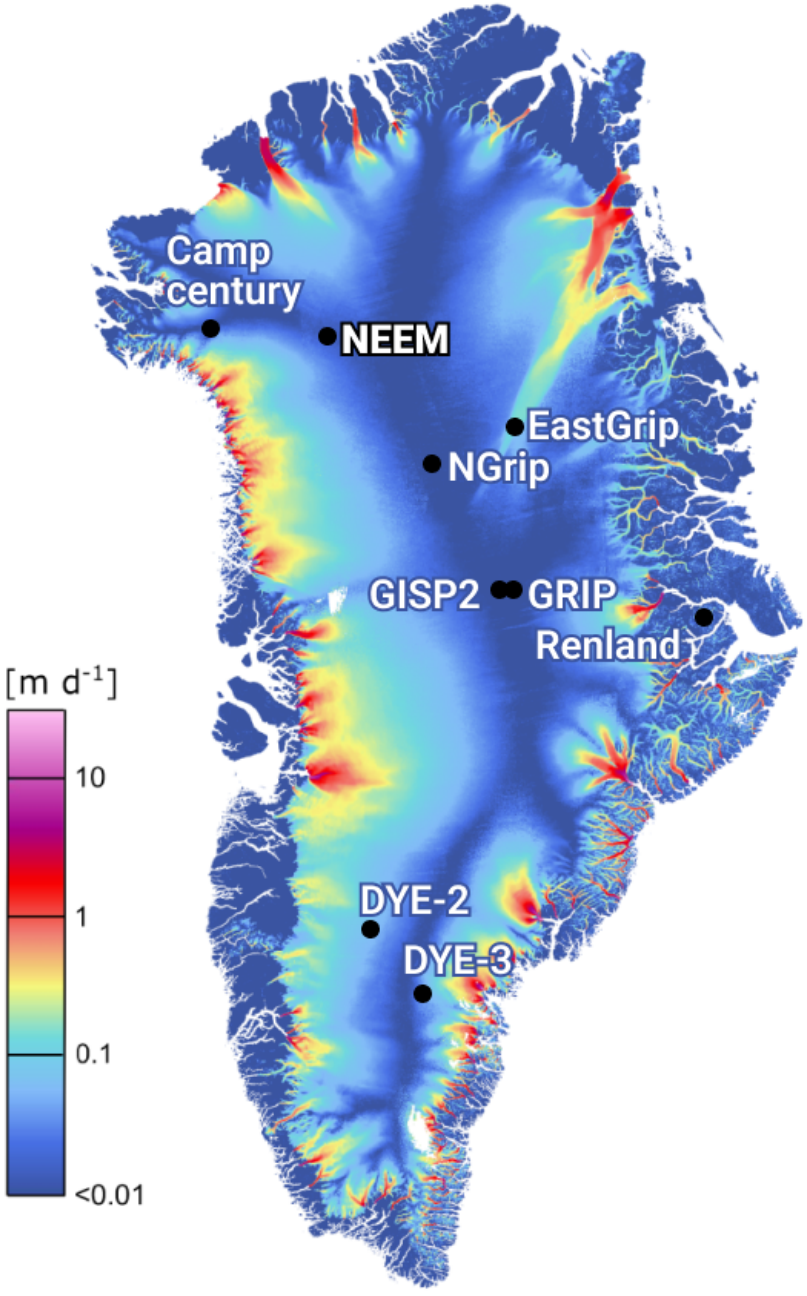

Figure 1. Greenland Ice Sheet velocity map from Sentinel-1, winter campaign 2019/2020 [version 1.3], modified from Nagler et al. (2015). Locations of various Greenland ice core projects are indicated. NEEM and most deep cores are positioned in areas of thicker ice with low horizontal flow (e.g., NEEM at 5.8 m/year (Hvidberg et al., 2012)) to capture undisturbed stratigraphy for paleoclimate reconstruction. In contrast, the EastGRIP site, situated on the Northeast Greenland Ice Stream, experiences much faster flow (50 m/year) and is the first deep core site focused on studying ice properties and flow dynamics (Hvidberg et al., 2020).

https://doi.org/10.5194/egusphere-2025-3647
Preprint. Discussion started: 26 September 2025

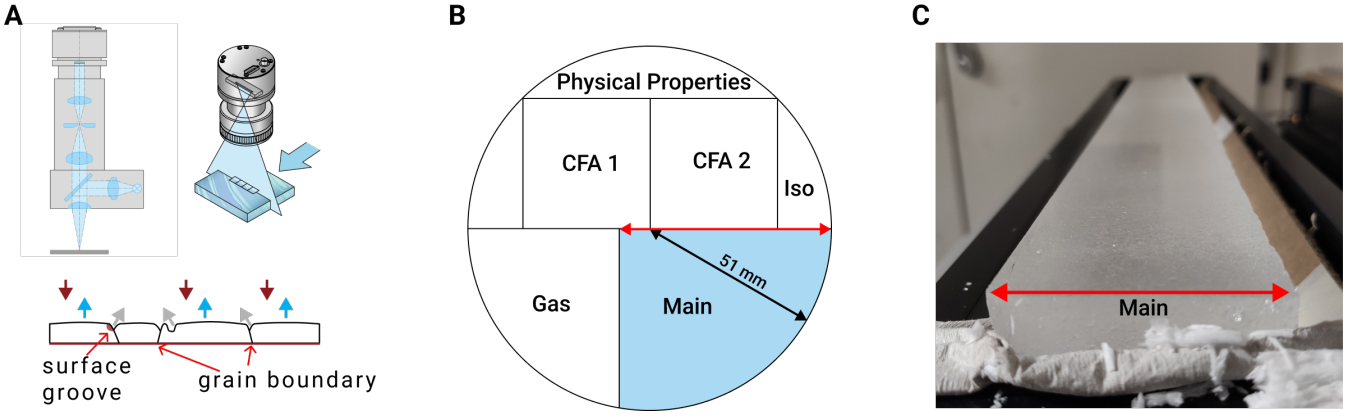

Figure 2. (A) Diagram of the xLASM's illumination setup, showing the line-scanning mechanism with a schematic of bright-field illumination, where light reflects from the polished ice surface and away in grooves or boundaries. (B) The NEEM ice core sampling scheme with the section analysed in this study is highlighted in blue. Figure adapted from Vasileios Gkinis et al. (2021). (C) Photograph of the NEEM ice core half-cylinder (main piece) mounted in the ice core carrier, prepared for scanning.

2 Methods

The NEEM project (2008-2012) drilled a 2540 m ice core in northwest Greenland, designed to provide a complete record of the Eemian interglacial period and earlier glacial stages, thus addressing questions about Greenland's ice sheet stability during warmer climates (Dahl-Jensen et al., 2013). The study focuses on the ice microstructure evolution through the abrupt glacial-interglacial events GI-19.2, GS-20, and GI-20. We analyse depths from 2004 m to 2020 m, which captures the glacial period GS-20 and its transitions into and out of the surrounding interglacial periods. The new c-axis data, specifically from depths of 2009 m to 2015 m, were provided by the Alfred Wegener Institute (personal communication, Ilka Weikusat, AWI). Immediately after drilling, the NEEM ice core samples were stored below -20°C. During transport, the cores were maintained in a continuously sub-zero environment, shipped frozen from Greenland to Kangerlussuaq, and then to permanent archives in Copenhagen, where they were subsequently stored in freezers set at -27°C.

2.1 Microstructure mapping

In this study, we present a novel extra Large Area Scanning Microscope (xLASM) to capture high-resolution images of ice microstructure. The xLASM setup incorporates a 3-axis system and a line-scan camera with 8192 pixels, achieving a resolution of 5 microns per pixel (Krischke et al., 2015). The xLASM directs a laser beam onto the polished and sublimated ice surface (Figure 2A), measuring the intensity of reflected light to distinguish structural features. Undisturbed surfaces reflect light with high intensity and appear bright in the image, while grain defects, such as grain boundaries, scatter light away from the sensor, resulting in darker regions.

https://doi.org/10.5194/egusphere-2025-3647
Preprint. Discussion started: 26 September 2025

Before imaging, we polished 55 cm-long ice core sections, or "bags", using an automated microtome. The microtome platform, designed to prepare up to 60 cm ice core sections, includes a fully automated setup that smooths semi-circular ice cores. Mounted on a granite surface plate for stability, the system uses a linear rail for precise motion, with an aluminium portal supporting the microtome blade. Stepper motors control horizontal and inclined vertical motions, ensuring high precision and repeatability.

The sampled sections were prepared according to the cutting scheme shown in Figure 2B, with the Main sections used in this study corresponding to archive sections (Figure 2C). After polishing, the sections were exposed to controlled sublimation at -20°C. This removes surface artefacts and enhances the visibility of microstructural features such as grain boundaries, subgrain grooves, and air bubbles.

The xLASM can scan sections up to 60 cm in length and 10 cm in width by scanning half-core sections in three overlapping runs, each covering 41 mm in width. These overlapping scans ensure comprehensive coverage and facilitate matching in the processing step. Scanning a 55 cm section typically takes about 5 minutes, producing high-resolution grayscale images approximately 400 MB in size per run. After imaging, the sections are returned to storage with <1 mm of ice removed from the surface during preparation.

Image Processing

Before processing, the raw images captured by the xLASM reveal distinct microstructural features directly from the sublimated ice surfaces. Figure 3 shows two representative sections of the NEEM ice core, highlighting differences in microstructure between glacial stadial and interstadial phases. Figure 3A (Bag 3661 at 2013.55 m depth) represents a glacial stadial section, displaying subhorizontal layering and cloudy bands associated with smaller grain sizes and higher impurity concentrations. In contrast, Figure 3B (Bag 3670 at 2018.5 m depth), representing an interstadial phase, exhibits features plate-like inclusions that serve as proxies for ice grain orientation, providing valuable context for understanding fabric patterns. Both images show bubbles at a depth where they would typically not be present, indicating relaxation effects. Gow (1971) describes how relaxation in deep ice occurs mainly as a result of the growth of bubble-like cavities and, to a lesser degree, to the formation of the previously mentioned plate-like inclusions propagated parallel to the basal planes of the ice grain. Additionally, intermediate line scanner observations on the NorthGrip and EastGrip cores show clear differences in the ice microstructure (Westhoff, 2021).

The measured digital images were processed using Python's Scikit-Image library (Van Der Walt et al., 2014), following three main phases: pre-processing, processing, and analysis:

- **Pre-processing:** We corrected lighting inconsistencies and sensor noise using adaptive histogram equalisation and Gaussian filtering. Regions of interest were selected manually, focusing on areas that exhibit microstructural complexity. By targeting sections with varied or intricate ice grain structures, we ensured the automated processing would account for the different features observed in the ice images.

https://doi.org/10.5194/egusphere-2025-3647
Preprint. Discussion started: 26 September 2025

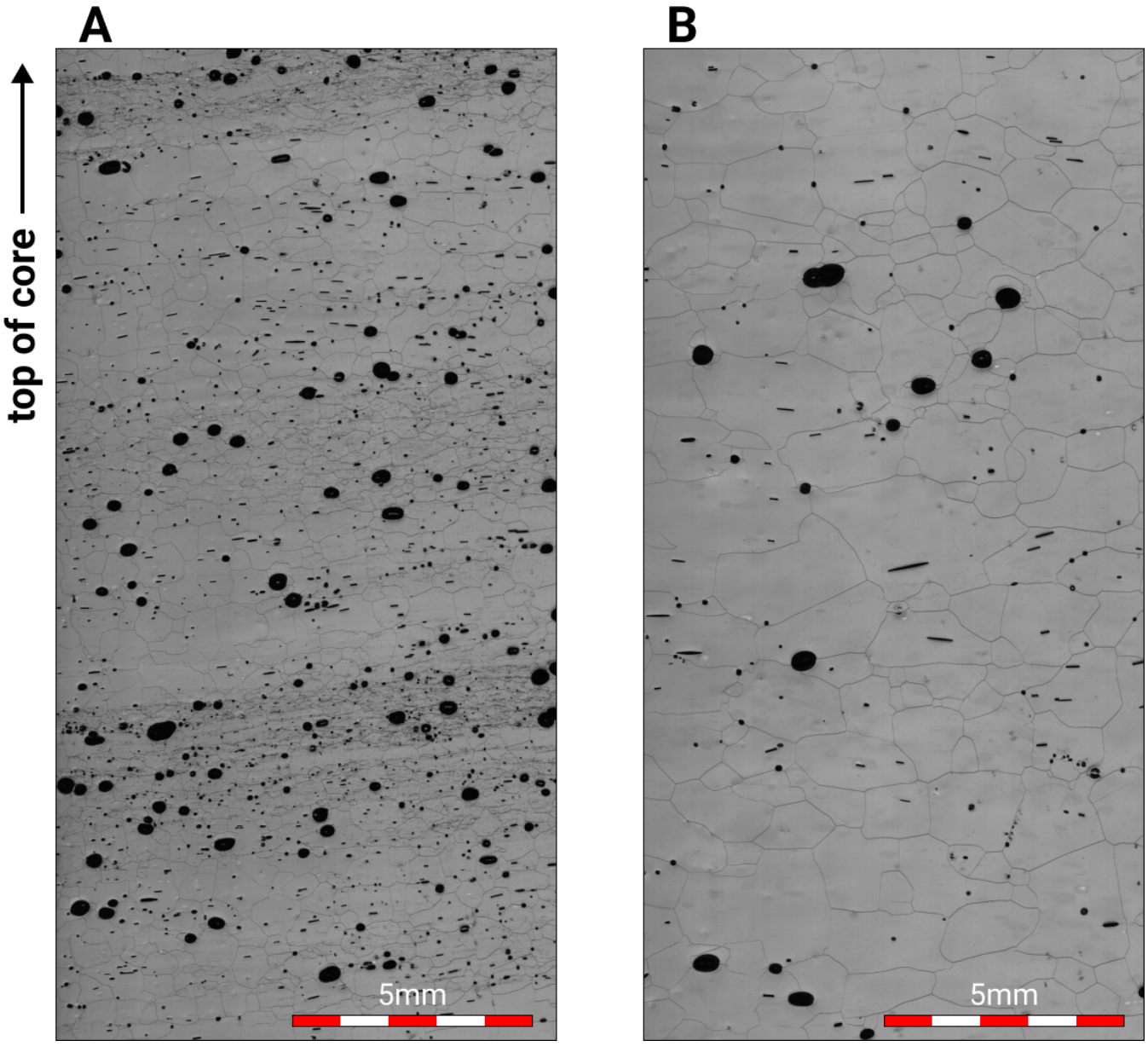

Figure 3. Sections of the NEEM ice core scanned by the xLASM. The sections were drilled in 2010 and scanned between 2022 and 2023. (A) Bag 3661 at depth 2013.55 m (from top). (B) Bag 3670 at 2018.5 m depth (from top). The sections correspond to the stadial and interstadial phases, respectively. Bubbles (black areas) present at this depth are dissociated hydrates now converted back to bubbles. The difference in the two sections arises from the higher impurity content load in bag 3661.

https://doi.org/10.5194/egusphere-2025-3647
Preprint. Discussion started: 26 September 2025

- **Processing:** Ridge operator algorithms were employed to identify ice grain boundaries. The Hessian filter was applied to capture etched boundaries, followed by noise reduction using scikit-image morphology tools.
- **Analysis:** Pixel-connected regions were labelled using scikit-image's label function, and morphological data were extracted with regionprops, providing metrics such as area, perimeter, and centroid.

2.2 Grain orientation and Fabric analysis

Fabric analysis is used to study the mechanical anisotropy of hexagonal ice, as the distribution of c-axis orientations evolves with depth. Here, we utilised c-axis orientation data derived from the automated Fabric Analyser G50 (AWI). The data combines measurements from established NEEM fabric datasets (Eichler et al., 2013; Montagnat et al., 2014) with several new measurements explicitly acquired for the detailed interval investigated in this study. The analysis methods are described in Montagnat et al. (2014); Wilson et al. (2003). This system captures high-resolution images of the ice fabric by using polarised light to measure the orientation of individual grains. The resulting data are represented through the eigenvalues e1, e2, and e3 of the second-order orientation tensor. The third eigenvalue (e3) indicates the primary concentration of the c-axis, while e1 and e2 describe the orthogonal directions of grain orientations with e3>e2>e1. These eigenvalues provide quantitative measures of fabric strength and orientation.

Shear Strain rate and Borehole logging

A logger is slowly lowered down through the borehole at 0.25 m/s and measures temperature, liquid pressure, diameter, inclination, and azimuth (Gundestrup et al., 1993). The logger is 1.8 m long and centred with callipers at the end, allowing a sufficient sampling of inclination and azimuth to reconstruct the shape of the borehole. Since reaching bedrock in 2010, the borehole logging has been operated on 17 July 2010, 21 July 2011, 25 May 2012, 10 May 2015, and 18 May 2019. From the inclination and azimuth, the shape of the borehole can be calculated for each of the borehole loggings. The change of horizontal velocity with depth or shear strain rate is determined by the difference in the shape of the borehole between the years (Dahl-Jensen et al., 1998) (Figure 4). As the study here is restricted to a zone of only 16 m, the stress field and ice temperature do not vary significantly, and the changing values of the shear strain rate can be attributed solely to other parameters, such as changes in ice grain properties, rheology, and impurity concentrations.

2.3 Water isotopes

The water isotopic data $\delta^{18}O_{ice}$ used in this study were obtained from the NEEM ice core, as published by Gkinis et al. (2021). This dataset provides ultra-high-resolution measurements at 0.05 m intervals, spanning approximately 120 kyr and capturing key climate events, including the Last Glacial Maximum and the Eemian interglacial. The isotopic analyses were conducted using Cavity Ring-Down Spectroscopy (CRDS), calibrated to the VSMOW-SLAP scale to ensure high precision and accuracy (Vasileios Gkinis et al., 2021).

https://doi.org/10.5194/egusphere-2025-3647
Preprint. Discussion started: 26 September 2025

2.4 Impurities and Continuous flow analysis

The impurity concentration data used in this study were obtained from continuous flow analysis (CFA) measurements on the NEEM ice core, as published by (Erhardt et al., 2022). This high-resolution dataset includes calcium (Ca^{2+}), sodium (Na^{+}), ammonium (NH_4^{+}), and nitrate (NO_3^{-}), recorded at resolutions of up to 1 mm. The CFA method provides near-continuous impurity profiles with minimised contamination risk, supporting the analysis of seasonal and sub-seasonal variability in ice cores.

3 Results

3.1 Grain Size and Climatic events

The grain size in the NEEM ice core exhibits a strong correlation with abrupt climatic transitions, distinctly marking shifts between stadial and interstadial periods. In Figure 4, covering the interval from 2004 to 2020 m depth, grain size closely follows the climatic temperature proxy ($\delta^{18}O$), with larger grains observed during interstadials and smaller grains during stadials. This pattern also extends to the aspect ratio, which reflects more elongated grains in stadial ice and more equant shapes in interstadial ice. The changes in grain size and aspect ratio align with the $\delta^{18}O$ variations, highlighting the link between ice microstructure and rapid climatic temperature shifts during deposition.

3.2 Fabric Orientation

Fabric orientation analysis indicates a stable crystal-preferred orientation (CPO) across the studied depths and the last glacial ice. The eigenvalues (e1, e2, and e3) shown in Figure 4 demonstrate this consistency, with e3 values around 0.9 and e2 and e1 values ranging between 0.01 and 0.03. These values reflect a high degree of anisotropy and a strongly preferred orientation. This strong clustering towards the vertical is visually confirmed by representative c-axis pole figures from different depths within and surrounding the main study interval (Figure 5).

3.3 Impurity Concentrations

Impurity concentrations in the NEEM ice core exhibit distinctive patterns corresponding to abrupt climatic events. During stadial periods, there is a marked increase in concentrations of calcium (Ca^{2+}), sodium (Na^{+}), ammonium (NH_4^{+}), and nitrate (NO_3^{-}) as depicted in Figure 4. Conversely, interstadial periods are characterised by reduced impurity concentrations, reflecting the cleaner atmospheric conditions associated with warmer climates.

3.4 Shear Strain Rate

Shear strain rate varies between stadial and interstadial ice, with higher rates generally associated with lower $\delta^{18}O$ values, smaller grains, and higher impurity concentrations. This trend suggests that impurity-rich ice experiences accelerated defor-

https://doi.org/10.5194/egusphere-2025-3647
Preprint. Discussion started: 26 September 2025

mation, correlating with the increased shear strain rate observed in these intervals. However, due to the low spatial resolution of borehole measurements, some abrupt climatic events may not be fully captured in the shear strain data.

4 Discussion

4.1 Grain size and abrupt events

The NEEM ice core data show a strong correlation between grain size and abrupt climatic transitions, with larger grains during interstadials and smaller grains in stadials, as seen in Figure 4. This pattern aligns with studies linking impurity-rich stadial layers to grain size reduction (Durand et al., 2006b) as the temperature change at the deposition time is long diffused (Løkkegaard et al., 2023). However, the mechanism remains complex. Previous NEEM studies, such as Eichler et al. (2017), observed that most impurities in NEEM ice are embedded within grains rather than at grain boundaries, making it unlikely that Zener pinning alone is responsible for grain size reduction. Instead, Eichler suggests that these inclusions may enhance recrystallisation dynamics indirectly under stress.

Further, Faria et al. (2014) proposed that dynamic recrystallisation, including grain growth, rotation, and strain-induced boundary migration, plays a central role in modulating grain size across depth. Laboratory studies also underscore that smaller grains can promote grain boundary sliding, facilitating deformation in fine-grained ice (Duval and Castelnau, 1995; Behn et al., 2021). These findings, coupled with the composite flow law model by Kuiper et al. (2020b), indicate that grain size-sensitive mechanisms likely accelerate deformation in impurity-rich, fine-grained stadial ice, reflecting the combined effects of impurities, recrystallisation, and stress.

4.2 Fabric Orientation and Climatic Stability

The fabric presents a strong single vertical maximum at a depth of 2004-2020 m, indicated by stable eigenvalues (e1, e2, e3), with e3 values consistently around 0.9, remaining stable across climatic transitions. Scatter plots of δ^{18}O against eigenvalues over 200 m and 400 m intervals (Figure 6) show no apparent correlation between fabric orientation and climate proxies, below the self-evident transition from compressional to simple shear stress and deformation regime described by Montagnat et al. (2014).

Despite impurity presence, this stability in fabric orientation is consistent with modelling studies showing that dislocation creep dominates c-axis fabric evolution under sustained ice sheet stress conditions, with minimal influence from dynamic recrystallisation mechanisms (Azuma, 1994; Llorens et al., 2016, 2017). The vertical anisotropy contributes to mechanical strength in the vertical direction and reflects the cumulative deformation history under simple shear stress at these depths, consistent with the strongly clustered c-axis fabric observed in the NEEM core(Montagnat et al., 2014). These results align with Wilson et al. (2014), who noted that fabric structure in polar ice reflects cumulative strain, remaining unaffected by short-term variations in temperature and impurity concentrations.

https://doi.org/10.5194/egusphere-2025-3647
Preprint. Discussion started: 26 September 2025

4.3 Impurity effects

Our results show strong negative correlations between grain size and impurity concentrations, particularly for Ca^{2+} (-0.78), dust (-0.74), and Na^{+} (-0.71) (Figure 7). These findings suggest higher impurity levels are generally associated with smaller grains, particularly in stadial ice. Given the non-normal distribution of grain size data, Spearman's rank correlation coefficient accommodates the monotonic relationships observed in the dataset (Hauke and Kossowski, 2011).

Literature studies on deep ice cores have shown that grain size variations closely track climatic transitions, with colder, impurity-rich stadial ice characterised by smaller grains and cleaner interstadial ice by larger grains (Thorsteinsson et al., 1995; Azuma et al., 2000; Durand et al., 2006b). This has been interpreted as the result of impurities inhibiting grain boundary migration, either through Zener pinning by insoluble dust particles (Weiss et al., 2002) or through a more diffuse reduction in grain boundary mobility. Recent studies suggest that direct particle pinning may play a limited role in polar ice, and that the bulk effect of soluble and insoluble impurities on boundary mobility is a more likely mechanism (Eichler et al., 2017; Stoll et al., 2021). Our observations at NEEM show strong anticorrelations between grain size and impurity concentration without direct evidence of particle-boundary pinning, which is consistent with this interpretation.

4.4 Shear Strain Rate and Ice Dynamics

Shear strain rates in the NEEM ice core vary significantly with climatic periods, showing higher rates in impurity-rich, fine-grained stadial ice. This increase in strain rate during stadials likely results from the combined effects of smaller grain sizes and elevated impurity concentrations, both of which facilitate deformation through grain size-sensitive creep. Notably, the ice grain orientations remain unchanged throughout the event. To investigate whether minor variations within the stable fabric could still influence the mechanical response, VPFFT simulations were performed on samples from the GS-20/GI-20 transition (Figure 4). The modelling indicates a relatively homogeneous mechanical response that is insensitive to minor spatial variations in fabric orientation within the samples, and also shows comparable bulk behaviour between the adjacent glacial and interglacial ice, despite slight fabric differences (Figure 8). This supports the interpretation that the observed stability of the strong c-axis fabric reflects a mechanical state robust to minor fluctuations in this regime. This is the first study where deformation rates, detailed grain properties, and orientations are made over a strong and clear DO event spanning only 16 m. Over such a small distance, the temperature, temperature history, and stress field do not change significantly, so we can conclude that grain size or impurity concentration, which is strongly linked to grain size, causes significant changes in shear strain deformation. Constitutive equations thus need to include a term to explain changes in ice grain properties, alongside terms related to ice temperature and ice grain orientation. Few attempts have been made to formulate constitutive equations that include ice grain size (Kuiper et al., 2020a, b) before the shear strain rate was fully measured.

https://doi.org/10.5194/egusphere-2025-3647
Preprint. Discussion started: 26 September 2025

5 Conclusion

In this study, we introduce the first dataset acquired using the xLASM, which enables non-destructive analysis of semicircular ice core sections without requiring thin-section preparation. By integrating the xLASM with an automated microtome, we achieved continuous scanning of 55 cm ice core segments, producing detailed insights into the microstructural features of the NEEM ice core and providing a high-resolution analysis across a Dansgaard-Oeschger (DO) event.

Our findings reveal strong correlations between grain size, impurity concentrations, and shear deformation rates across different climatic periods, underscoring the responsiveness of ice microstructures to abrupt climatic shifts. The observed fabric orientation remains consistent despite changes in impurity levels, suggesting that long-term deformation history predominantly governs fabric evolution over short-term variations in impurity content.

Code availability. he Python scripts used for image processing and data analysis are available at: https://doi.org/10.5281/zenodo.15356797.

Author contributions. MM designed the study, performed the data analysis, and wrote the manuscript with input from all co-authors. AL and SK developed the laboratory setup and methodology. IW and SK provided fabric data and contributed to the discussion. YH and SK acquired the xLASM data, and YH developed parts of the Python processing code. MGL provided feedback on the discussion, fabric data, and VPFFT modelling to complement the data analysis. DDJ contributed to the study design, provided borehole data, and gave feedback on the manuscript. All authors contributed to the interpretation of the results and approved the final manuscript.

Competing interests. The authors declare that they have no competing interests.

Acknowledgements. This project has received funding from the European Union's Horizon 2020 research and innovation programme under the Marie Skłodowska-Curie grant agreement No 955750

https://doi.org/10.5194/egusphere-2025-3647
Preprint. Discussion started: 26 September 2025

References

Azuma, N.: A Flow Law for Anisotropic Ice and Its Application to Ice Sheets, Earth and Planetary Science Letters, 128, 601–614, https://doi.org/10.1016/0012-821X(94)90173-2, 1994.

Azuma, N., Wang, Y., Yoshida, Y., Narita, H., Hondoh, T., Shoji, H., and Watanabe, O.: Crystallographic Analysis of the Dome Fuji Ice Core, Physics of Ice Core Records, pp. 45–61, 2000.

Baker, I., Cullen, D., and Iliescu, D.: The Microstructural Location of Impurities in Ice, Canadian Journal of Physics, 81, 1–9, https://doi.org/10.1139/p03-030, 2003.

Barnes, P. R. and Wolff, E. W.: Distribution of Soluble Impurities in Cold Glacial Ice, Journal of Glaciology, 50, 311–324, https://doi.org/10.3189/172756504781829918, 2004.

Behn, M. D., Goldsby, D. L., and Hirth, G.: The Role of Grain Size Evolution in the Rheology of Ice: Implications for Reconciling Laboratory Creep Data and the Glen Flow Law, The Cryosphere, 15, 4589–4605, https://doi.org/10.5194/tc-15-4589-2021, 2021.

Binder, T.: Measurements of Grain Boundary Networks in Deep Polar Ice Cores - A Digital Image Processing Approach, Ph.D. thesis, Universitätsbibliothek Heidelberg, 2014.

Binder, T., Garbe, C., Wagenbach, D., Freitag, J., and Kipfstuhl, S.: Extraction and Parametrization of Grain Boundary Networks in Glacier Ice, Using a Dedicated Method of Automatic Image Analysis: EXTRACTION AND PARAMETRIZATION OF GRAIN BOUNDARY NETWORKS, Journal of Microscopy, 250, 130–141, https://doi.org/10/f4sgx8, 2013.

Dahl-Jensen, D., Thorsteinsson, T., Alley, R., and Shoji, H.: Flow Properties of the Ice from the Greenland Ice Core Project Ice Core: The Reason for Folds?, Journal of Geophysical Research: Oceans, 102, 26 831–26 840, https://doi.org/10.1029/97JC01266, 1997.

Dahl-Jensen, D., Mosegaard, K., Gundestrup, N., Clow, G. D., Johnsen, S. J., Hansen, A. W., and Balling, N.: Past Temperatures Directly from the Greenland Ice Sheet, Science, 282, 268–271, 1998.

Dahl-Jensen, D., Albert, M. R., Aldahan, A., Azuma, N., Balslev-Clausen, D., Baumgartner, M., Berggren, A.-M., Bigler, M., Binder, T., Blunier, T., Bourgeois, J. C., Brook, E. J., Buchardt, S. L., Buizert, C., Capron, E., Chappellaz, J., Chung, J., Clausen, H. B., Cvijanovic, I., Davies, S. M., Ditlevsen, P., Eicher, O., Fischer, H., Fisher, D. A., Fleet, L. G., Gfeller, G., Gkinis, V., Gogineni, S., Goto-Azuma, K., Grinsted, A., Gudlaugsdottir, H., Guillevic, M., Hansen, S. B., Hansson, M., Hirabayashi, M., Hong, S., Hur, S. D., Huybrechts, P., Hvidberg, C. S., Iizuka, Y., Jenk, T., Johnsen, S. J., Jones, T. R., Jouzel, J., Karlsson, N. B., Kawamura, K., Keegan, K., Kettner, E., Kipfstuhl, S., Kjær, H. A., Koutnik, M., Kuramoto, T., Köhler, P., Laepple, T., Landais, A., Langen, P. L., Larsen, L. B., Leuenberger, D., Leuenberger, M., Leuschen, C., Li, J., Lipenkov, V., Martinerie, P., Maselli, O. J., Masson-Delmotte, V., McConnell, J. R., Miller, H., Mini, O., Miyamoto, A., Montagnat-Rentier, M., Mulvaney, R., Muscheler, R., Orsi, A. J., Paden, J., Panton, C., Pattyn, F., Petit, J.-R., Pol, K., Popp, T., Possnert, G., Prié, F., Prokopiou, M., Quiquet, A., Rasmussen, S. O., Raynaud, D., Ren, J., Reutenauer, C., Ritz, C., Röckmann, T., Rosen, J. L., Rubino, M., Rybak, O., Samyn, D., Sapart, C. J., Schilt, A., Schmidt, A. M. Z., Schwander, J., Schüpbach, S., Seierstad, I., Severinghaus, J. P., Sheldon, S., Simonsen, S. B., Sjolte, J., Solgaard, A. M., Sowers, T., Sperlich, P., Steen-Larsen, H. C., Steffen, K., Steffensen, J. P., Steinhage, D., Stocker, T. F., Stowasser, C., Sturevik, A. S., Sturges, W. T., Sveinbjörnsdottir, A., Svensson, A., Tison, J.-L., Uetake, J., Vallelonga, P., van de Wal, R. S. W., van der Wel, G., Vaughn, B. H., Vinther, B., Waddington, E., Wegner, A., Weikusat, I., White, J. W. C., Wilhelms, F., Winstrup, M., Witrant, E., Wolff, E. W., Xiao, C., Zheng, J., and NEEM community members: Eemian Interglacial Reconstructed from a Greenland Folded Ice Core, Nature, 493, 489–494, https://doi.org/10.1038/nature11789, 2013.

https://doi.org/10.5194/egusphere-2025-3647
Preprint. Discussion started: 26 September 2025

Dansgaard, W., Johnsen, S. J., Clausen, H. B., Dahl-Jensen, D., Gundestrup, N. S., Hammer, C. U., Hvidberg, C. S., Steffensen, J. P., Sveinbjörnsdottir, A. E., Jouzel, J., and Bond, G.: Evidence for General Instability of Past Climate from a 250-Kyr Ice-Core Record, Nature, 364, 218–220, https://doi.org/10.1038/364218a0, 1993.

Durand, G., Gagliardini, O., Thorsteinsson, T., Svensson, A., Kipfstuhl, S., and Dahl-Jensen, D.: Ice Microstructure and Fabric: An up-to-Date Approach for Measuring Textures, Journal of Glaciology, 52, 619–630, https://doi.org/10.3189/172756506781828377, 2006a.

Durand, G., Weiss, J., Lipenkov, V., Barnola, J. M., Krinner, G., Parrenin, F., Delmonte, B., Ritz, C., Duval, P., Röthlisberger, R., and Bigler, M.: Effect of Impurities on Grain Growth in Cold Ice Sheets, Journal of Geophysical Research, 111, F01 015, https://doi.org/10/fc8f7z, 2006b.

Duval, P. and Castelnau, O.: Dynamic Recrystallization of Ice in Polar Ice Sheets, Le Journal de Physique IV, 05, C3–197–C3–205, https://doi.org/10.1051/jp4:1995317, 1995.

Duval, P., Ashby, M. F., and Anderman, I.: Rate-Controlling Processes in the Creep of Polycrystalline Ice, The Journal of Physical Chemistry, 87, 4066–4074, https://doi.org/10.1021/j100244a014, 1983.

Eichler, J., Weikusat, I., and Kipfstuhl, S.: C-Axis Fabric Analysis of Ice Samples Collected from the NEEM Ice Core, https://doi.org/10.1594/PANGAEA.838063, 2013.

Eichler, J., Kleitz, I., Bayer-Giraldi, M., Jansen, D., Kipfstuhl, S., Shigeyama, W., Weikusat, C., and Weikusat, I.: Location and Distribution of Micro-Inclusions in the EDML and NEEM Ice Cores Using Optical Microscopy and in Situ Raman Spectroscopy, The Cryosphere, 11, 1075–1090, https://doi.org/10.5194/tc-11-1075-2017, 2017.

Erhardt, T., Bigler, M., Federer, U., Gfeller, G., Leuenberger, D., Stowasser, O., Röthlisberger, R., Schüpbach, S., Ruth, U., Twarloh, B., Wegner, A., Goto-Azuma, K., Kuramoto, T., Kjær, H. A., Vallelonga, P. T., Siggaard-Andersen, M.-L., Hansson, M. E., Benton, A. K., Fleet, L. G., Mulvaney, R., Thomas, E. R., Abram, N., Stocker, T. F., and Fischer, H.: High-Resolution Aerosol Concentration Data from the Greenland NorthGRIP and NEEM Deep Ice Cores, Earth System Science Data, 14, 1215–1231, https://doi.org/10.5194/essd-14-1215-2022, 2022.

Faria, S. H., Weikusat, I., and Azuma, N.: The Microstructure of Polar Ice. Part II: State of the Art, Journal of Structural Geology, 61, 21–49, https://doi.org/10/gmqk4w, 2014.

Glen: The Creep of Polycrystalline Ice, Proceedings of the Royal Society of London. Series A. Mathematical and Physical Sciences, 228, 519–538, https://doi.org/10.1098/rspa.1955.0066, 1955.

Glen, J. W.: Experiments on the Deformation of Ice, Journal of Glaciology, 2, 111–114, https://doi.org/10.3189/S0022143000034067, 1952.

Goldsby, D. L. and Kohlstedt, D. L.: Superplastic Deformation of Ice: Experimental Observations, Journal of Geophysical Research: Solid Earth, 106, 11 017–11 030, https://doi.org/10.1029/2000JB900336, 2001.

Gow, A. J.: Relaxation of Ice in Deep Drill Cores from Antarctica, Journal of Geophysical Research, 76, 2533–2541, https://doi.org/10.1029/JB076i011p02533, 1971.

Grootes, P. M., Stuiver, M., White, J. W. C., Johnsen, S., and Jouzel, J.: Comparison of Oxygen Isotope Records from the GISP2 and GRIP Greenland Ice Cores, Nature, 366, 552–554, https://doi.org/10.1038/366552a0, 1993.

Gundestrup, N., Dahl-Jensen, D., Johnsen, S., and Rossi, A.: Bore-Hole Survey at Dome GRIP 1991, Cold Regions Science and Technology, 21, 399–402, https://doi.org/10.1016/0165-232X(93)90015-Z, 1993.

Hammonds, K. and Baker, I.: The Effects of Ca^{++} on the Strength of Polycrystalline Ice, Journal of Glaciology, 62, 954–962, https://doi.org/10.1017/jog.2016.84, 2016.

https://doi.org/10.5194/egusphere-2025-3647
Preprint. Discussion started: 26 September 2025

Hansen, B. L. and Langway, C. C.: Deep Core Drilling in Ice and Core Analysis at Camp Century, Greenland, 1961-66, Antarctic Journal of the United States, 1, 207–208, 1966.

Hauke, J. and Kossowski, T.: Comparison of Values of Pearson's and Spearman's Correlation Coefficients on the Same Sets of Data, QUAGEO, 30, 87–93, https://doi.org/10.2478/v10117-011-0021-1, 2011.

Hvidberg, C., Larsen, L., Dahl-Jensen, D., and Buchardt, S.: Surface movement and elevation change at the NEEM deep drilling site, North Greenland, 2007-2011, in: EGU General Assembly Conference Abstracts, vol. 14, p. 12101, 2012.

Hvidberg, C. S., Grinsted, A., Dahl-Jensen, D., Khan, S. A., Kusk, A., Andersen, J. K., Neckel, N., Solgaard, A., Karlsson, N. B., Kjær, H. A., and Vallelonga, P.: Surface Velocity of the Northeast Greenland Ice Stream (NEGIS): Assessment of Interior Velocities Derived from Satellite Data by GPS, The Cryosphere, 14, 3487–3502, https://doi.org/10.5194/tc-14-3487-2020, 2020.

Iliescu, D. and Baker, I.: Effects of Impurities and Their Redistribution during Recrystallization of Ice Crystals, Journal of Glaciology, 54, 362–370, https://doi.org/10.3189/002214308784886216, 2008.

Jacka, T. and Jun, L.: The Steady-State Crystal Size of Deforming Ice, Annals of Glaciology, 20, 13–18, https://doi.org/10.3189/1994AoG20-1-13-18, 1994.

Jacka, T. H.: Laboratory Studies on Relationships between Ice Crystal Size and Flow Rate, Cold Regions Science and Technology, 10, 31–42, https://doi.org/10.1016/0165-232X(84)90031-4, 1984.

Kipfstuhl, S., Weikusat, I., Lambrecht, A., Freitag, J., Faria, S., Grigoriev, D., and Azuma, N.: Microstructure Mapping: A New Method for Imaging Deformation-Induced Microstructural Features of Ice on the Grain Scale, Journal of Glaciology - J GLACIOLOGY, 52, https://doi.org/10/crkqpr, 2006.

Krischke, A., Oechsner, U., and Kipfstuhl, S.: Rapid Microstructure Analysis of Polar Ice Cores: Analyzing Past Climates Using the Large Area Scan Macroscope, Optik & Photonik, 10, 32–35, https://doi.org/10/f27ch3, 2015.

Kuiper, E.-J. N., De Bresser, J. H. P., Drury, M. R., Eichler, J., Pennock, G. M., and Weikusat, I.: Using a Composite Flow Law to Model Deformation in the NEEM Deep Ice Core, Greenland – Part 2: The Role of Grain Size and Premelting on Ice Deformation at High Homologous Temperature, The Cryosphere, 14, 2449–2467, https://doi.org/10.5194/tc-14-2449-2020, 2020a.

Kuiper, E.-J. N., Weikusat, I., De Bresser, J. H. P., Jansen, D., Pennock, G. M., and Drury, M. R.: Using a Composite Flow Law to Model Deformation in the NEEM Deep Ice Core, Greenland – Part 1: The Role of Grain Size and Grain Size Distribution on Deformation of the Upper 2207 m, The Cryosphere, 14, 2429–2448, https://doi.org/10.5194/tc-14-2429-2020, 2020b.

Llorens, M.-G., Griera, A., Bons, P. D., Lebensohn, R. A., Evans, L. A., Jansen, D., and Weikusat, I.: Full-field predictions of ice dynamic recrystallisation under simple shear conditions, Earth and Planetary Science Letters, 450, 233–242, https://doi.org/10.1016/j.epsl.2016.06.045, 2016.

Llorens, M.-G., Griera, A., Steinbach, F., Bons, P. D., Gomez-Rivas, E., Jansen, D., Roessiger, J., Lebensohn, R. A., and Weikusat, I.: Dynamic Recrystallization during Deformation of Polycrystalline Ice: Insights from Numerical Simulations, Philosophical Transactions of the Royal Society A: Mathematical, Physical and Engineering Sciences, 375, 20150 346, https://doi.org/10.1098/rsta.2015.0346, 2017.

Løkkegaard, A., Mankoff, K. D., Zdanowicz, C., Clow, G. D., Lüthi, M. P., Doyle, S. H., Thomsen, H. H., Fisher, D., Harper, J., Aschwanden, A., Vinther, B. M., Dahl-Jensen, D., Zekollari, H., Meierbachtol, T., McDowell, I., Humphrey, N., Solgaard, A., Karlsson, N. B., Khan, S. A., Hills, B., Law, R., Hubbard, B., Christoffersen, P., Jacquemart, M., Seguinot, J., Fausto, R. S., and Colgan, W. T.: Greenland and Canadian Arctic Ice Temperature Profiles Database, The Cryosphere, 17, 3829–3845, https://doi.org/10.5194/tc-17-3829-2023, 2023.

https://doi.org/10.5194/egusphere-2025-3647
Preprint. Discussion started: 26 September 2025

Montagnat, M., Azuma, N., Dahl-Jensen, D., Eichler, J., Fujita, S., Gillet-Chaulet, F., Kipfstuhl, S., Samyn, D., Svensson, A., and Weikusat, I.: Fabric along the NEEM Ice Core, Greenland, and Its Comparison with GRIP and NGRIP Ice Cores, The Cryosphere, 8, 1129–1138, https://doi.org/10.5194/tc-8-1129-2014, 2014.

Nagler, T., Rott, H., Hetzenecker, M., Wuite, J., and Potin, P.: The Sentinel-1 Mission: New Opportunities for Ice Sheet Observations, Remote Sensing, 7, 9371–9389, https://doi.org/10.3390/rs70709371, 2015.

North Greenland Ice Core Project members: High-Resolution Record of Northern Hemisphere Climate Extending into the Last Interglacial Period, Nature, 431, 147–151, https://doi.org/10.1038/nature02805, 2004.

Nye, J. F.: The Distribution of Stress and Velocity in Glaciers and Ice-Sheets, Proceedings of the Royal Society of London. Series A. Mathematical and Physical Sciences, 239, 113–133, https://doi.org/10.1098/rspa.1957.0026, 1957.

Obbard, R. and Baker, I.: The Microstructure of Meteoric Ice from Vostok, Antarctica, Journal of Glaciology, 53, 41–62, https://doi.org/10.3189/172756507781833901, 2007.

Otosaka, I. N., Shepherd, A., Ivins, E. R., Schlegel, N.-J., Amory, C., Van Den Broeke, M., Horwath, M., Joughin, I., King, M., Krinner, G., Nowicki, S., Payne, T., Rignot, E., Scambos, T., Simon, K. M., Smith, B., Sandberg Sørensen, L., Velicogna, I., Whitehouse, P., A, G., Agosta, C., Ahlstrøm, A. P., Blazquez, A., Colgan, W., Engdahl, M., Fettweis, X., Forsberg, R., Gallée, H., Gardner, A., Gilbert, L., Gourmelen, N., Groh, A., Gunter, B. C., Harig, C., Helm, V., Khan, S. A., Konrad, H., Langen, P., Lecavalier, B., Liang, C.-C., Loomis, B., McMillan, M., Melini, D., Mernild, S. H., Mottram, R., Mouginot, J., Nilsson, J., Noël, B., Pattle, M. E., Peltier, W. R., Pie, N., Sasgen, I., Save, H., Seo, K.-W., Scheuchl, B., Schrama, E., Schröder, L., Simonsen, S. B., Slater, T., Spada, G., Sutterley, T., Vishwakarma, B. D., Van Wessem, J. M., Wiese, D., Van Der Wal, W., and Wouters, B.: Mass Balance of the Greenland and Antarctic Ice Sheets from 1992 to 2020, https://doi.org/10.5194/essd-2022-261, 2022.

Pimienta, P., Duval, P., and Lipenkov, V. Y.: Mechanical Behavior of Ice Along the 2040 m Vostok Core, Antarctica, Annals of Glaciology, 10, 137–140, https://doi.org/10.3189/S0260305500004316, 1988.

Rhodes, R. H., Baker, J. A., Millet, M.-A., and Bertler, N. A.: Experimental Investigation of the Effects of Mineral Dust on the Reproducibility and Accuracy of Ice Core Trace Element Analyses, Chemical Geology, p. S0009254111001938, https://doi.org/10.1016/j.chemgeo.2011.05.006, 2011.

Stoll, N., Eichler, J., Hörhold, M., Shigeyama, W., and Weikusat, I.: A Review of the Microstructural Location of Impurities in Polar Ice and Their Impacts on Deformation, Frontiers in Earth Science, 8, 2021.

Thorsteinsson, T., Kipfstuhl, J., Eicken, H., Johnsen, S. J., and Fuhrer, K.: Crystal size variations in Eemian-age ice from the GRIP ice core, Central Greenland, Earth and Planetary Science Letters, 131, 381–394, https://doi.org/10.1016/0012-821X(95)00031-7, 1995.

Van Der Walt, S., Schönberger, J. L., Nunez-Iglesias, J., Boulogne, F., Warner, J. D., Yager, N., Gouillart, E., and Yu, T.: Scikit-Image: Image Processing in Python, PeerJ, 2, e453, https://doi.org/10.7717/peerj.453, 2014.

Vasileios Gkinis, Bo M. Vinther, Trevor J. Popp, Thea Quistgaard, Anne-Katrine Faber, Christian T. Holme, Camilla-Marie Jensen, Mika Lanzky, Anine-Maria Lütt, Vasileios Mandrakis, Niels-Ole Ørum, Anna-Sofie Pedersen, Nikol Vaxevani, Yongbiao Weng, Emilie Capron, Dorthe Dahl-Jensen, Maria Hörhold, Tyler R. Jones, Jean Jouzel, Amaëlle Landais, Valérie Masson-Delmotte, Hans Oerter, Sune O. Rasmussen, Hans Christian Steen-Larsen, Jørgen-Peder Steffensen, Árný-Erla Sveinbjörnsdóttir, Anders Svensson, Bruce Vaughn, and James W. C. White: A 120,000-Year Long Climate Record from a NW-Greenland Deep Ice Core at Ultra-High Resolution, Scientific Data, 8, 141, https://doi.org/10.1038/s41597-021-00916-9, 2021.

Weikusat, I., Kipfstuhl, S., Faria, S. H., Azuma, N., and Miyamoto, A.: Subgrain Boundaries and Related Microstructural Features in EDML (Antarctica) Deep Ice Core, Journal of Glaciology, 55, 461–472, https://doi.org/10.3189/002214309788816614, 2009.

https://doi.org/10.5194/egusphere-2025-3647
Preprint. Discussion started: 26 September 2025

Weikusat, I., Miyamoto, A., Faria, S. H., Kipfstuhl, S., Azuma, N., and Hondoh, T.: Subgrain Boundaries in Antarctic Ice Quantified by X-ray Laue Diffraction, Journal of Glaciology, 57, 111–120, https://doi.org/10.3189/002214311795306628, 2011.

Weiss, J., Vidot, J., Gay, M., Arnaud, L., Duval, P., and Petit, J. R.: Dome Concordia Ice Microstructure: Impurities Effect on Grain Growth, Annals of Glaciology, 35, 552–558, https://doi.org/10.3189/172756402781816573, 2002.

Westhoff, J.: Visual Stratigraphy of the EastGRIP Ice Core. Of the Lost Ice Core Orientation, Deformation Structures, Extreme Warm Events, and Trapped Ancient Air., Thesis, University of Copenahgen, Copenhagen, 2021.

Wilson, C. J., Peternell, M., Piazolo, S., and Luzin, V.: Microstructure and Fabric Development in Ice: Lessons Learned from in Situ Experiments and Implications for Understanding Rock Evolution, Journal of Structural Geology, 61, 50–77, https://doi.org/10.1016/j.jsg.2013.05.006, 2014.

Wilson, C. J. L., Russell-Head, D. S., and Sim, H. M.: The Application of an Automated Fabric Analyzer System to the Textural Evolution of Folded Ice Layers in Shear Zones, Annals of Glaciology, 37, 7–17, https://doi.org/10.3189/172756403781815401, 2003.

https://doi.org/10.5194/egusphere-2025-3647
Preprint. Discussion started: 26 September 2025

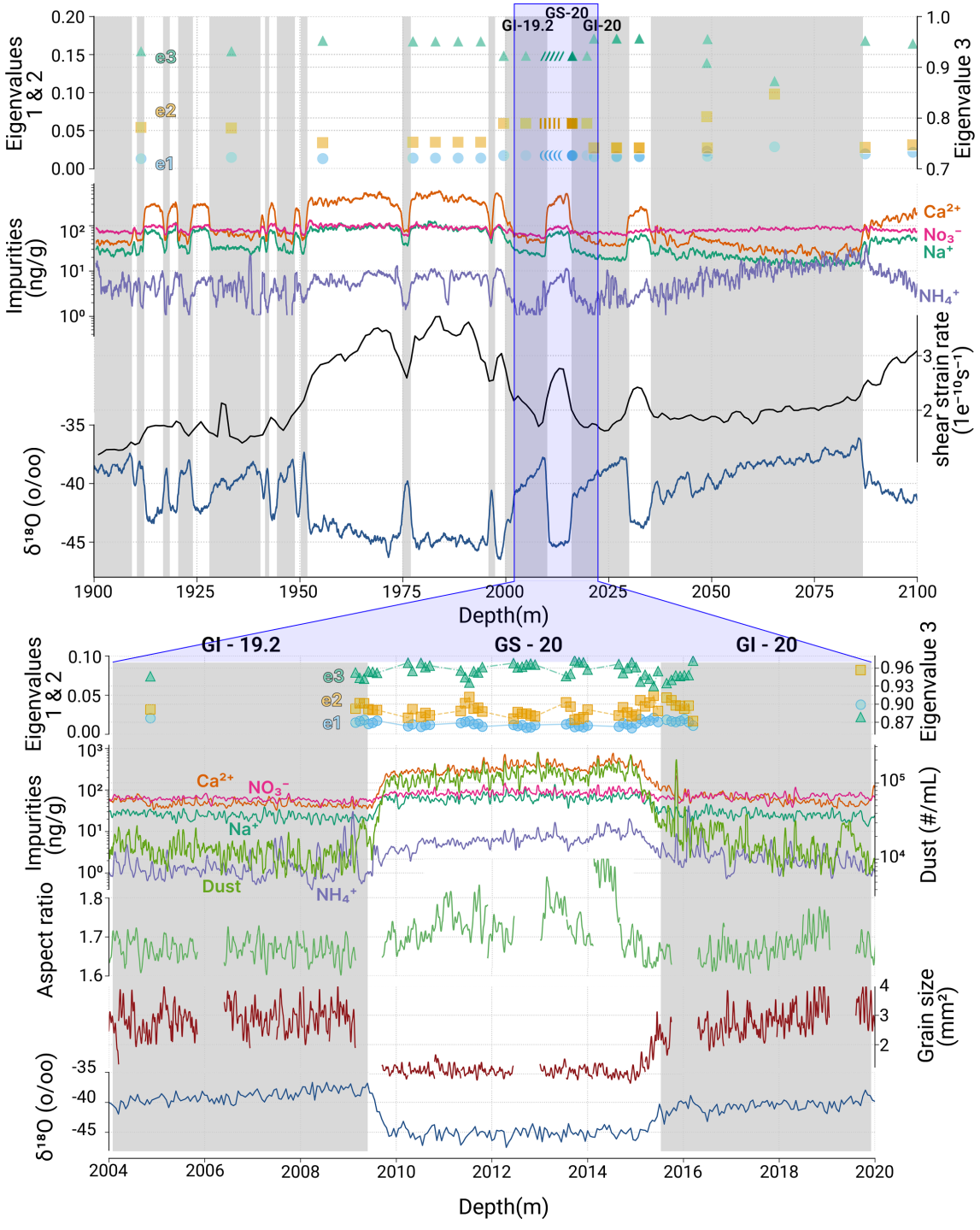

Figure 4. Top frame: Variations in grain size and profiles of stable water isotopes ($\delta^{18}O$), shear strain rate, impurity concentrations (Ca^{2+}, conductivity, dust, Na^+, NH_4^+, and NO_3^-), and fabric eigenvalues (e1, e2, e3) across 1900 to 2100 m depth in the NEEM ice core. Bottom frame: The same parameters except for shear strain rate across 2004 to 2020 m. The data illustrate parameter responses to abrupt climatic transitions, showing distinct changes, particularly in impurity concentrations, as the ice shifts from stadial to interstadial periods. Notably, fabric orientation remains stable across these events, as indicated by consistent eigenvalues.

https://doi.org/10.5194/egusphere-2025-3647
Preprint. Discussion started: 26 September 2025

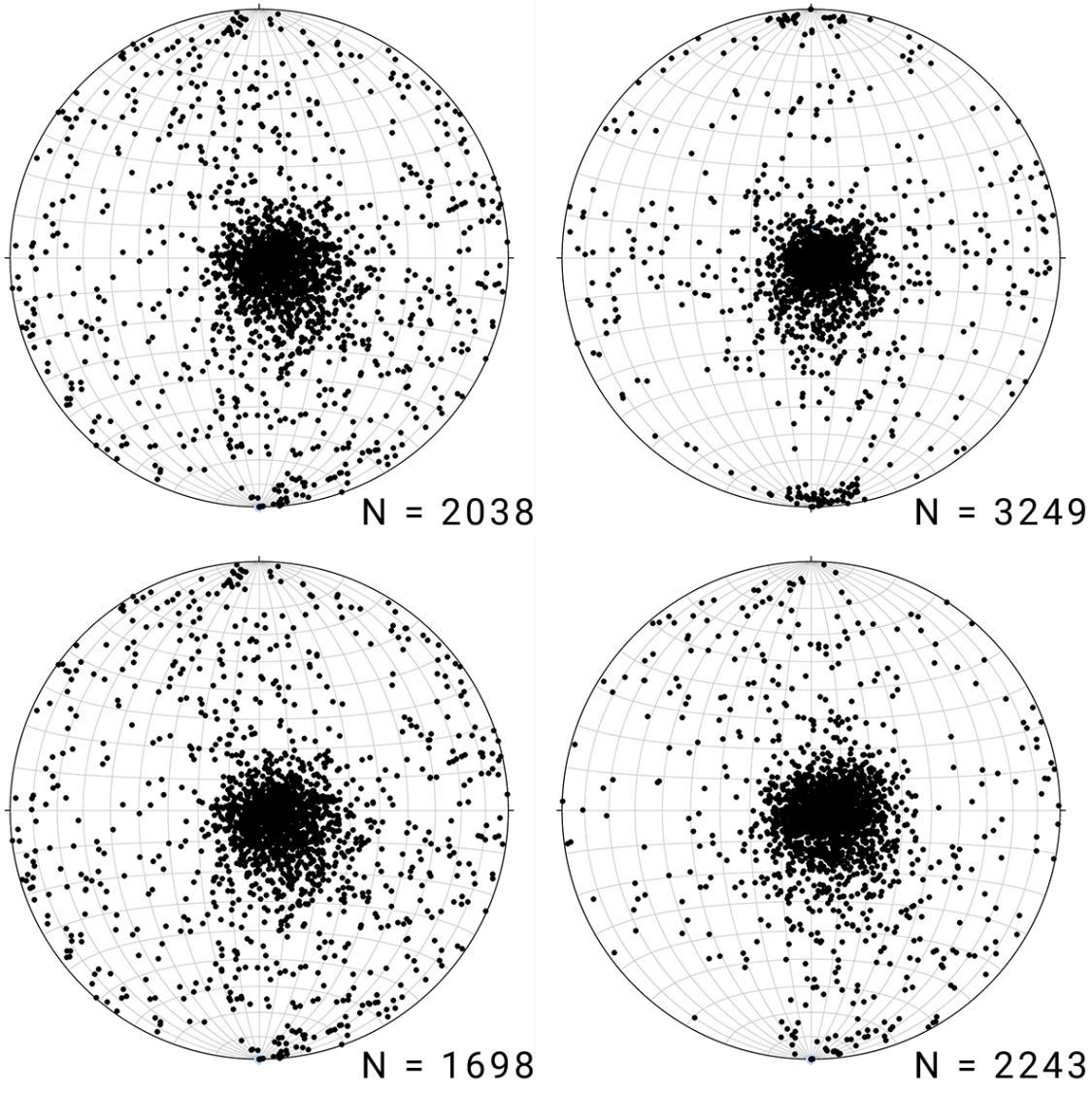

Figure 5. Representative c-axis orientation fabrics from NEEM ice core samples, plotted as Schmidt equal-area, lower hemisphere projections. The plots show data from bag 3626 (top left, 2004 m depth, N=2038 grains), bag 3646 (top right, 2014 m depth, N=3249 grains), bag 3673 (bottom left, 2020 m depth, N=1698 grains), and bag 3696 (bottom right, 2032 m depth, N=2243 grains). All samples exhibit a strong single maximum cluster, consistent with the high e3 eigenvalues presented in Figure 4 and typical for NEEM ice at these depths under shear deformation.

https://doi.org/10.5194/egusphere-2025-3647
Preprint. Discussion started: 26 September 2025

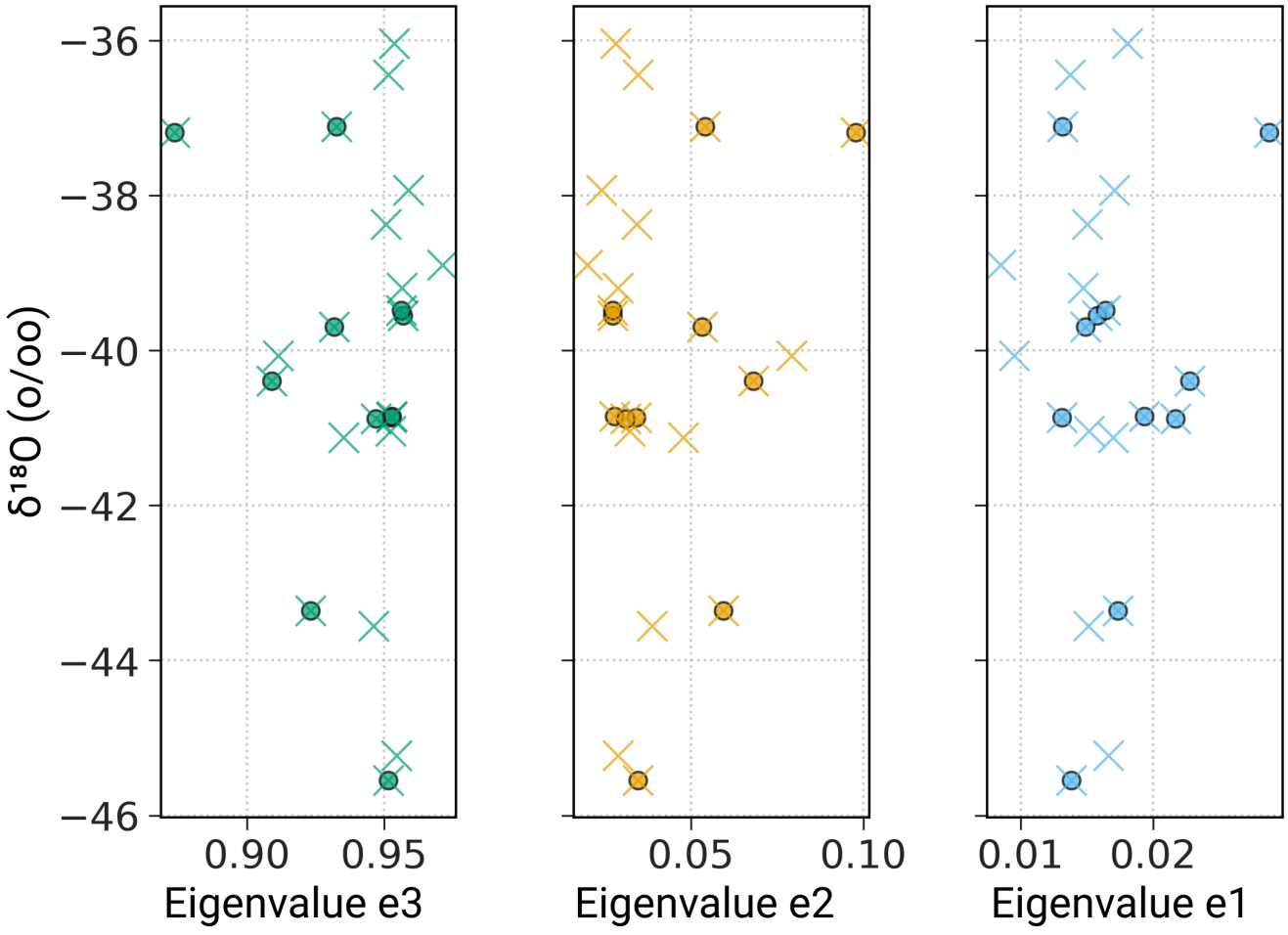

Figure 6. Scatter plots showing the relationship between δ^{18}O (vertical axis) and fabric eigenvalues (e1, e2, and e3 on the horizontal axis) at two different depth intervals in the NEEM ice core: 1700-2100 m (solid circles) and 1900-2100 m (crosses). The lack of clear trends or clustering across these intervals suggests no significant correlation between δ^{18}O values and fabric orientation, supporting the interpretation that fabric evolution is predominantly driven by long-term deformation rather than abrupt climatic events.

https://doi.org/10.5194/egusphere-2025-3647
Preprint. Discussion started: 26 September 2025

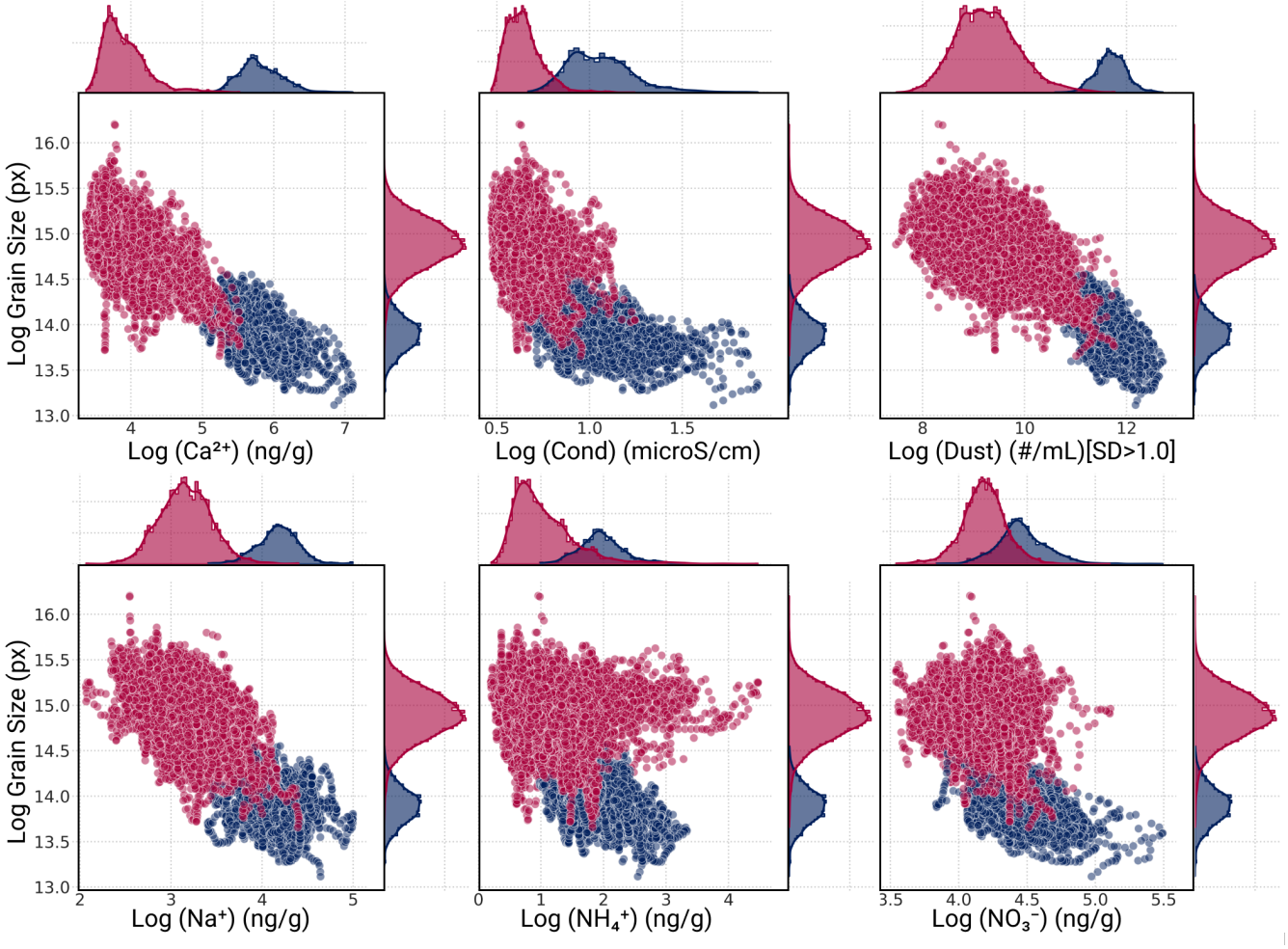

Figure 7. log-log scatter plots of impurity concentrations (Ca^{2+}, conductivity, dust, Na^{+}, NH_4^{+}, and NO_3^{-}) versus grain size, with red data points indicating interstadial periods and blue data points indicating stadial periods. The histograms illustrate the distribution of impurity concentrations and grain sizes. The scatter plots show a negative correlation between impurity levels and grain size, with higher impurity concentrations associated with smaller grain sizes, particularly during stadial periods.

https://doi.org/10.5194/egusphere-2025-3647
Preprint. Discussion started: 26 September 2025

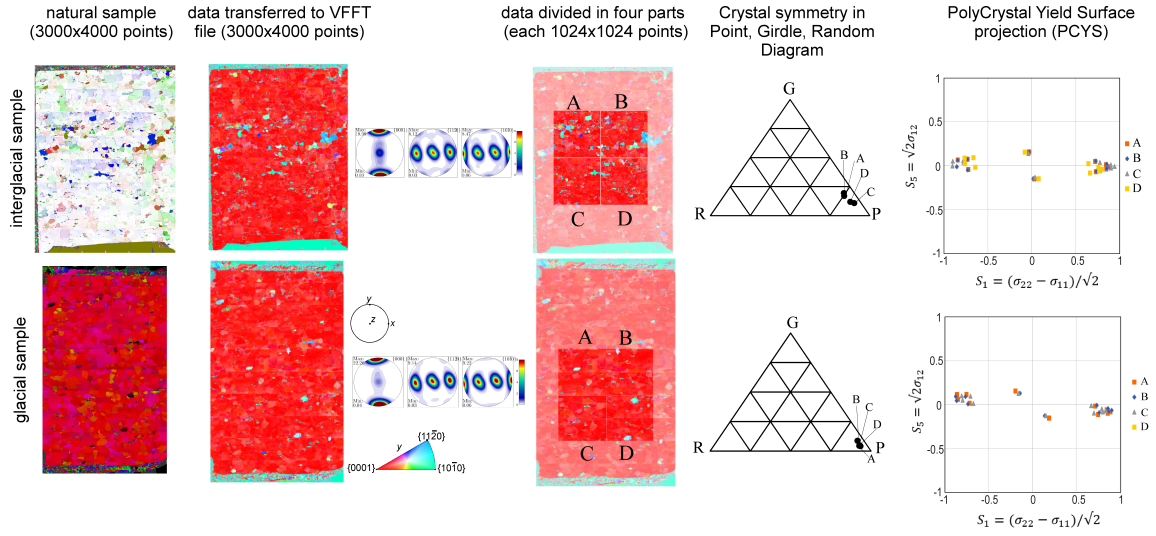

Figure 8. Visco-Plastic Fast Fourier Transform (VPFFT) modelling of adjacent interglacial (top row) and glacial (bottom row) samples from NEEM bag 3665 (2015.75 m depth, corresponding to the GS-20/GI-20 transition shown in Figure 4). Columns show (from left to right): optical image of the natural sample section; fabric data transferred to the VPFFT simulation grid (3000x4000 points); the sample section divided into four subregions (A, B, C, D, each 1024x1024 points) for homogeneity analysis; crystal symmetry representation confirming a strong cluster fabric (P: point, G: girdle, R: random); and the resulting Polycrystal Yield Surface (PCYS) projection under shear ($s_1 = (\sigma_{22} - \sigma_{11})/\sqrt{2}$ vs $s_5 = \sqrt{2}\sigma_{12}$). The close clustering of PCYS points for subregions A, B, C, and D (indicated by different symbols and colours) in both the interglacial and glacial samples suggests a relatively homogeneous mechanical response, despite micro-scale fabric variations and slight differences between the two samples. Modelling and figure courtesy of G. Llorens.